Journal of the Australian Ceramic Society (2022) 58:891–899
https://doi.org/10.1007/s41779-022-00740-3

RESEARCH

Effect of Y_2O_3 doping on a gehlenite/magnesia-alumina spinel obtained by sintering secondary aluminium ash

Yong Zhang[1] · Tiantian Duan[1] · Xiaojuan He[1] · Yuncai He[1] · Yuting Wang[1]

Received: 3 November 2021 / Revised: 19 March 2022 / Accepted: 2 April 2022 / Published online: 27 April 2022

Abstract

Due to the rapid development of China's regeneration industry, secondary aluminium ash (SAA) has been extensively produced. The reuse of SAA and Y_2O_3 doping was studied in this research. This proved that SAA can turn into a raw material for gehlenite/magnesia-alumina spinels. Furthermore, doping with Y_2O_3 can aggrandize the densification feature of gehlenite/magnesia-alumina spinels. The densification of the gehlenite/magnesia-alumina spinel without Y_2O_3 was lower than that of the doped spinel in the temperature range of 1573 to 1773 K. At 1673 K, 3 wt% Y_2O_3 was added to the gehlenite/magnesia-alumina spinel. It had a density of 2.05 g·cm^{-3} and a compressive strength of 91.2 MPa. Generally, 3 wt% Y_2O_3 was added, and the sintering temperature at 1673 K was appropriate. The elevation of the densification feature was also attributable to the solubility of Y_2O_3 and the formation of a low-viscosity liquid phase such as $YCaAl_3O_7$. The SAA can be reused for the recovery of gehlenite/magnesia-alumina spinels. Doping it with Y_2O_3 can broaden its reutilization in new water-resistant ceramic materials.

Keywords Secondary aluminium ash (SAA) · Sintering · Gehlenite/magnesia-alumina · Y_2O_3 · Doping

Introduction

Dregs of aluminium ash have already been popularly produced in China because the aluminium industry has grown. Nevertheless, in a landfill, over 90% of secondary aluminium ash (SAA) is handled without deeper management. In the natural environment, the negative influence of environmental quality has increased over the past few years [1, 2], and it is meaningful to recycle and reduce SAA. Al, $MgAl_2O_4$ (MA) spinels, and corundum are the major compounds of SAA. SAA uses minimal types of additional reagents with low costs that can be used as a raw material for spinels [3, 4]. There are many advantages of magnesium aluminium spinels, including a high melting point, mechanical properties, strong thermal and spalling properties, and excellent chemical performance. These characteristics make MA a main material for many adhibition applications in furnaces. It is necessary to use lining materials for the base and sidewall of the furnace [3]. However, the preparation of magnesium aluminate spinels is still an expensive process and should be supported by high-spirited and new technical techniques, which would lower the cost of raw materials and improve the quality of the outcome.

According to the characteristics of secondary aluminium ash raw materials, the ingredients can be slightly changed to prepare refractory materials [5, 6]. This can realize resource utilization. In recent years, to prepare a lightweight refractory material with both refractory properties (high strength) and reduced mass, the USA, Japan, and other countries successively developed phases that combine with melilite with a high melting point [7, 8]. MA is a kind of magnesium aluminium oxide material with a high melting point (2408 K), good thermal shock resistance, impact resistance, good electrical insulation performance, and strong alkali erosion resistance [9, 10]. Melilite is a class of silicate minerals that are composed of Al, Mg, and iron calcium silicate/sodium silicate, and its general chemical composition formula is $(Ca, Na)_2(Al, Mg, Fe)[(Al, Si)SiO_7]$. Gehlenite ($Ca_2Al_2SiO_7$ (C_2AS)) and akermanite ($Ca_2Mg(Si_2O_7)$) are two important minerals in the melilite group. Melilite has a low density, a small thermal expansion coefficient, and a low thermal conductivity. Melilite is rarely the main crystal phase of

✉ Yong Zhang
752607795@qq.com

[1] College of Land Resources and Environment, Jiangxi Agricultural University, Nanchang 330045, People's Republic of China

refractory materials because its melting point is not very high, but in improving the compressive strength and hydration resistance of materials, it has a vital function [11]. In conclusion, we can prepare refractory materials in which the main crystal phase is a magnesia-alumina spinel and the combined phase is melilite from secondary aluminium. If the result holds up, the potential harm of secondary aluminium ash to the environment can be reduced, and the field of refractory preparation can also be broadened.

Rare earth oxides (REOs) are valid annexing agents that have been diffusely used in chinaware, biotechnology, powder metallurgy, new energy, and chemical technology. WC-MgO bulk composites are doped with La_2O_3. The flexural strength and Vickers hardness are enhanced [12]. CeO_2 is one of the most reactive rare earth metal oxides and has some features, such as a large surface area, a large radius, and strong chemical resistance. It has been widely applied in conformational ceramics, such as oxide and nonoxide ceramics and functional ceramics [13, 14]. WC-Al_2O_3 compounds adulterated with 0.1% CeO_2 showed a fining microstructure and enhanced machine capability compared with nondoped composites [15]. Different scholars have studied the improved sinterability of high-quality spinels doped with 5 wt% Y_2O_3 [16, 17]. Sintering was found to be improved by using rare earth oxides such as 4 wt% Yb_2O_3 and Dy_2O_3 [18]. Densification of the specimens with Y_2O_3 and Nd_2O_3 was attributed to the formation of complex oxides, which activated the crystal lattice [19]. La_2O_3 and CeO_2 formed a liquid phase, which accelerated the densification of the crystal lattice [19]. The grain boundary energies decreased when the spinel was doped with 3 mol% Y_2O_3, Gd_2O_3, and La_2O_3 from grain boundary restraint detection [20].

In this work, the series of objectives were as follows. A gehlenite/magnesia-alumina spinel was synthesized from SAA. The effects of Y_2O_3 doping on the gehlenite/magnesia-alumina spinel were characterized. The mechanisms of densification improvement by Y_2O_3 doping on the gehlenite/magnesia-alumina spinel obtained from SAA were evaluated.

Experimental procedure

Materials

In Jiangxi Province, China, we collected secondary aluminium ash (SAA). The ash was preprocessed by drying, selection, and ball milling to obtain a uniform particle size. Repeated impact during the ball-milling process resulted in a large number of microscopic defects, such as lattice distortions, dislocations, twinned crystal structures, and strain energy in the powders [21]. The mineral phases of the ash were Al, α-Al_2O_3, MA, and AlN (Fig. 1). Chemical phase analysis showed that Al and α-Al_2O_3 accounted for 23.67 wt% and 23.57 wt% of the ash, respectively, with 2.19 wt% AlN and 9.10 wt% MA (Table 1). The analytical grade agents used for analysis and detection included CaO, MgO, and Y_2O_3.

Experiment

After disposal, the D_{50} of SAA was 23.42 μm. In this study, SAA (70.8 wt%) was blended with CaO (18.58 wt%) and MgO (10.62 wt%) in a mixing machine for 1 day. The powders were put into a mould with a 3% bonder at 15 MPa, and then, the powders were pressed into bricks (diameter of 2.5 cm and thickness of 1 cm). The raw bricks were placed in an electric stove for sintering in the range of 1373 to 1773 K for 3 h in air (Fig. 2). The sintering temperature curve of the experiment is shown in Fig. 3. The right and left sides of the stove were sealed with a quartz plug to keep the stove warm. The stove was cooled to 773 K at a rate of 3–4 K/min. The bricks were tested at room temperature. The addition amount was 3 wt% Y_2O_3. The mass fractions of SAA, CaO, MgO, and Y_2O_3 were 68.8%, 18.0%, 10.3%, and 2.9%, respectively.

Sample analysis

The surface microcosmic morphology of the powder was recorded by scanning electron microscopy (SEM, Nova NanoSEN 230). X-ray diffraction (XRD, TRAX, Rigaku) was employed using a Cu Kα radiation source and a 10°/min scanning speed to analyse the crystal structures of the

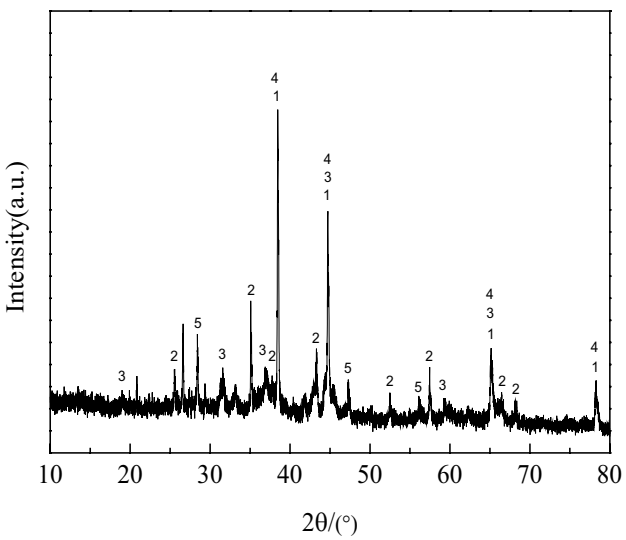

Fig. 1 XRD pattern of the SAA. 1-Al; 2-a-Al_2O_3; 3-$MgAl_2O_4$; 4-AlN; 5-ZnS

Table 1 Chemical composition of the SAA (wt%)

Composition	Al	Mg	Si	Ca	Fe	Na	Ti	Others
Content	39.61	6.39	7.26	3.47	1.20	1.03	1.61	39.43

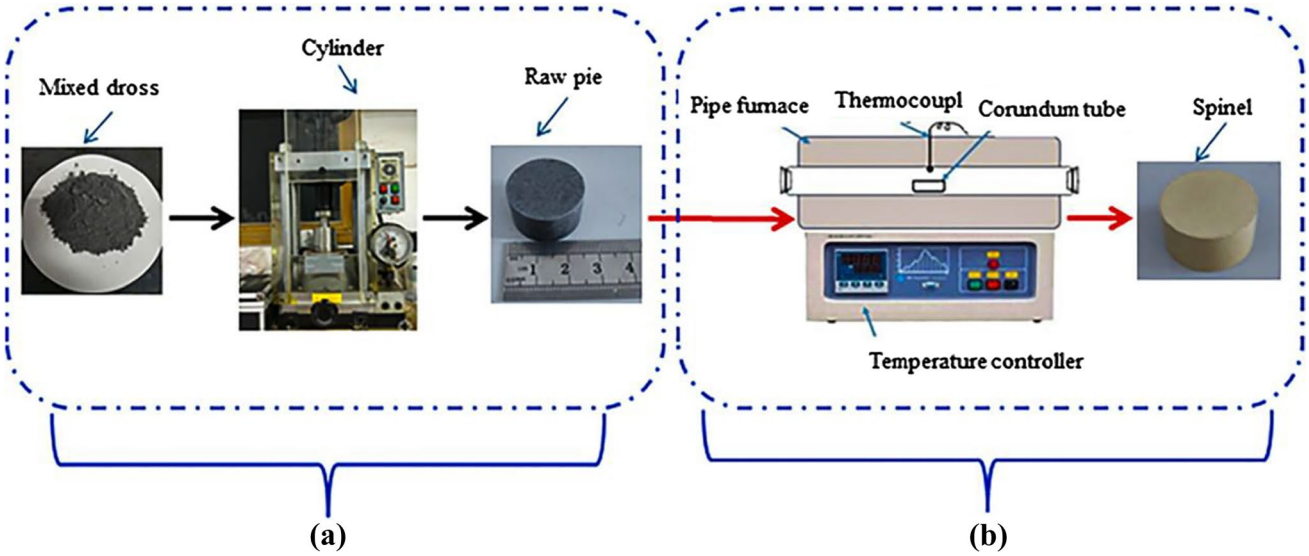

Fig. 2 Schematics of the spinel prepared by SAA: **a** moulding process and **b** sintering process

powders. The particle size distribution was examined by a laser particle analyser (OMEC LS-POP, China). The elements in SAA were examined by X-ray fluorescence (XRF-AXIOS, PANalytical, Netherlands). The powders were placed in a hydraulic press (YLJ-40 T, China) to obtain bricks. The compression strength was examined by an electrohydraulic compression machine (TYA-100C, China). The bulk density of the bricks was calculated using the Archimedes principle.

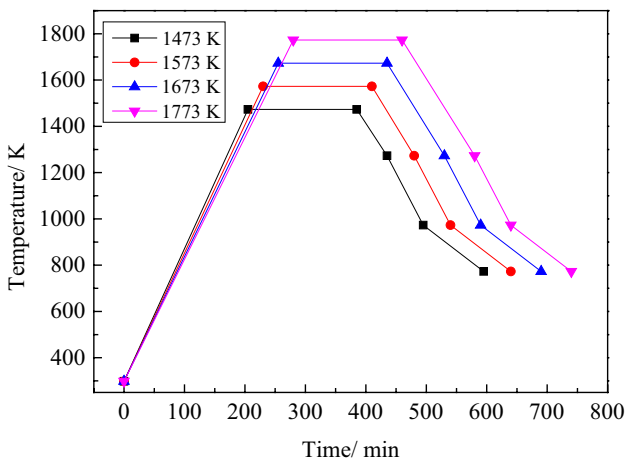

Fig. 3 Sintering temperature curve of the experiment

Results and discussion

Effect of sintering temperature on the characteristics of the gehlenite/magnesia-alumina spinel

The XRD patterns of the gehlenite/magnesia-alumina spinel from SAA at different sintering temperatures are shown in Fig. 4. The main phases in the spinel were C_2AS and MA in the temperature range of 1373 to 1773 K and C_2AS, MA, and Al_2O_3 at 1373 K. The crossover of SiO_2 enhanced the incorporation of the framework with the MA stroma. The silica compositions began to melt at a high temperature, and the liquid phase formed. SiO_2 softened and turned into a liquid amorphous glass phase. The liquid sintering process is due to the enhanced wetting between particles [22]. From XRD analysis, the main crystalline phases were C_2AS and MA. However, Al_2O_3 disappeared at 1473–1773 K. During the sintering process, the mass transfer was accelerated because of the liquid phase [23]. The results showed that CaO and SiO_2 could easily be turned into the liquid phase. CaO and SiO_2 allowed densification by recrystallization in the presence of the liquid phase [23]. The intensities of C_2AS and MA were slightly different at 1673 K and 1773 K.

The microstructures of gehlenite/magnesia-alumina spinel powders sintered at 1473–1773 K were shown (Fig. 5).

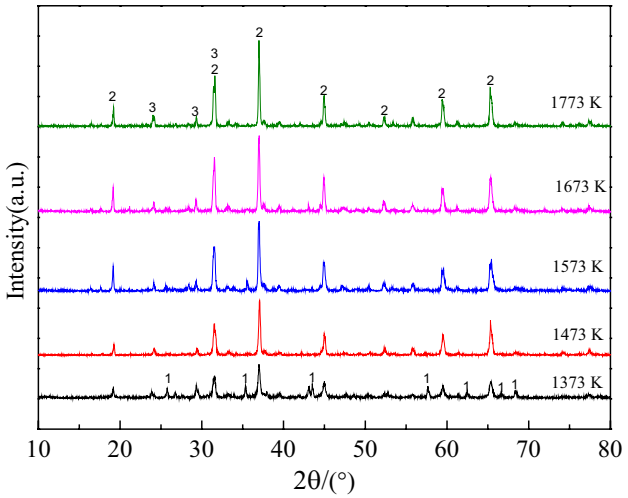

Fig. 4 XRD patterns of the gehlenite/magnesia-alumina spinel at different temperatures. 1-Al_2O_3; 2-$MgAl_2O_4$; 3-$Ca_2Al_2SiO_7$

From Fig. 5 (a–d), the grains were breezed tiny at 1473 K for 3 h. The grain boundary size of C_2AS and MA turned obviously with an increase in temperature to 1673 K. Likeness, from Fig. 5 (c–d), the crystalline grains were homogenous. And the MA linked another as the main phase at 1673 K. The main phase of the C_2AS was a big square plate. The products were with little compact and homogeneous microstructures at 1773 K. So the 1673 K was appropriated. In all specimens, a glassy phase appeared, which was mainly due to the liquid glassy phase. The CaO and SiO_2 components in the SAA decreased the viscosity of the glass phase, and that was good for the gehlenite/magnesia-alumina spinel synthesized during the course [24].

Effect of Y_2O_3 on the gehlenite/magnesia-alumina spinel

The grain boundaries were observable from the microstructure of the powders with 3 wt% Y_2O_3 (Fig. 6). By forming a brittle phase because of Y_2O_3, new grain propagation occurred. The crystallite dimension was larger and clearer than that of the spinel without Y_2O_3. The grain size increases became obvious upon doping with Y_2O_3. Finally, the grain dimension distribution was more uniform and enlarged with 3 wt% Y_2O_3. Figure 6 shows the microstructure of the gehlenite/magnesia-alumina bricks with 3 wt% Y_2O_3 at 1473–1773 K. EDS (Table 2) and line scan analysis (Fig. 6) showed that Y was uniformly dispersed in the texting scope. The average length of elongated grains increased with 3 wt% Y_2O_3. Y_2O_3 is a crystal phase regulator and improves the microstructure. Y_2O_3 addition influenced the densification and microstructure. The presence of $YCaAl_3O_7$ as a second phase could be beneficial as it influences grain growth and reduces ion segregation at grain boundaries. This may be the reason for the different microstructure refinement trends of ceramic particles shown in Fig. 6 and Fig. 5 [25].

From Fig. 7, the results showed the bulk density and compressive strength of the gehlenite/magnesia-alumina spinel with and without Y_2O_3 doping and upon sintering at 1373–1773 K. The density of the gehlenite/magnesia-alumina spinel increased to 2.03 g·cm^{-3} at 1773 K. The density of the gehlenite/magnesia-alumina spinel increased dramatically from 1.78 to 2.03 g·cm^{-3} as the temperature increased from 1373 to 1773 K. The density of the gehlenite/magnesia-alumina spinel increased mildly when the temperature was 1773 K (from 2.02 to 2.03 g·cm^{-3}). The compressive strength of the gehlenite/magnesia-alumina spinel also significantly increased from 69.1 to 75.2 MPa with an increase in temperature from 1373 to 1573 K, which was above the Chinese national standard value of 40 MPa for magnesia and magnesia-alumina refractory bricks (GB/T 2275–2007). When the temperature changed from 1673 to 1773 K, the compressive strength improved slightly from 89.8 to 90 MPa. This showed that 1673 K was suitable for synthesising gehlenite/magnesia-alumina.

In particular, the density feature of the Y_2O_3-doped gehlenite/magnesia-alumina spinel improved with sintering. The density of the gehlenite/magnesia-alumina spinel with 3 wt% Y_2O_3 was 2.05 g·cm^{-3} at 1673 K. The compressive strength of the gehlenite/magnesia-alumina spinel with 3 wt% Y_2O_3 showed a similar trend to the density trend. The compressive strengths of the samples doped with 3 wt% Y_2O_3 at 1373–1773 K reached 71.2, 75.7, 77.3, 91.2, and 92.3 MPa. The density and compressive strength of the Y_2O_3-doped gehlenite/magnesia-alumina spinel improved. Preparation of the Y_2O_3-doped gehlenite/magnesia-alumina spinel can expand the utilization of SAA in new ceramics.

Y_2O_3 can be the key factor in the densification of bricks because of the large ionic radius of the Y^{3+}. The glass network structure of the Y_2O_3 influenced the migration of other ions [19]. Y_2O_3 reacted with Al_2O_3, SiO_2, or CaO in SAA, and the outcome reinforced intergranular fracture with an increase in the sintering temperature. In addition, ions moved to the intergrain void as the temperature increased. The holes were filled completely, which effectively reduced the residual number of closed pores in the sample [26]. The densification feature of the bricks with Y_2O_3 was superior to that of the gehlenite/magnesia-alumina spinel without Y_2O_3 (above 1473 K).

Mechanism of enhanced sintering with Y_2O_3 for obtaining gehlenite/magnesia-alumina spinels

Reaction set

XRD patterns of the 3 wt% Y_2O_3 samples sintered at 1473–1773 K are shown in Fig. 8. Thus, from the XRD

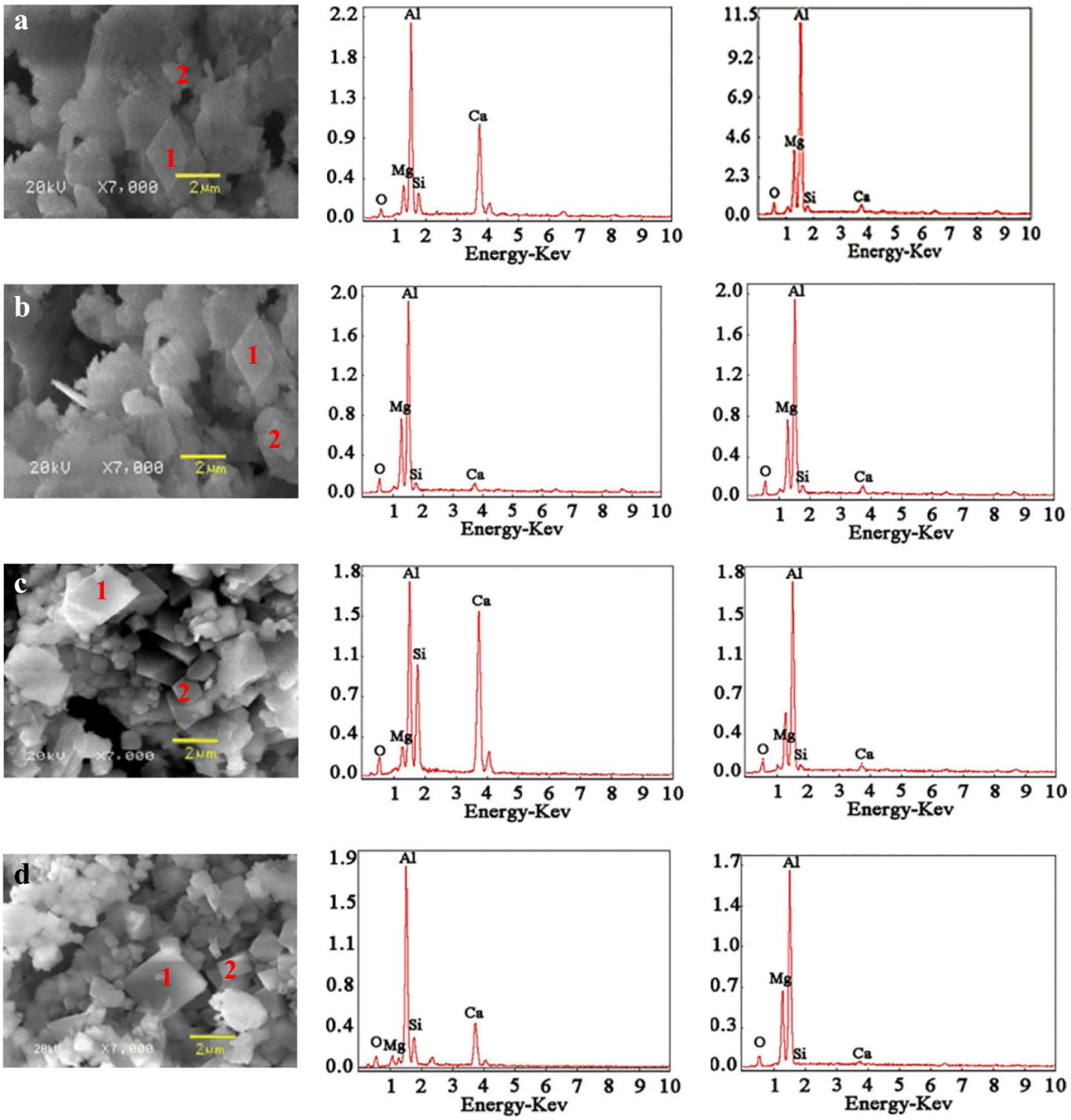

Fig. 5 SEM/EDS images of C_2AS/MA spinel powder at different sintering temperatures. **a** 1473 K; **b** 1573 K; **c** 1673 K; **d** 1773 K; 1 $Ca_2Al_2SiO_7$; 2 MA

analysis, the new compound that included Y ion was $YCaAl_3O_7$. The PDF card number of $YCaAl_3O_7$ is #49–0605. MA, C_2AS, and $YCaAl_3O_7$ were the main phases in the sintered product. Al_2O_3 was the minor phase at 1473 K. $YCaAl_3O_7$ appeared at 1473 K and existed from 1473 to 1773 K. A liquid phase during sintering was beneficial for the densification feature. The large cation size of Y^{3+} could have caused distortion between layers and an expanded lattice. The presence of $YCaAl_3O_7$ as a second phase could be beneficial by influencing grain growth and reducing ion segregation at grain boundaries. $YCaAl_3O_7$ exhibited well-elongated grains in the matrix between MA and C_2AS. $YCaAl_3O_7$ was helpful in the bonding of two or more MA and C_2AS particles [25, 27].

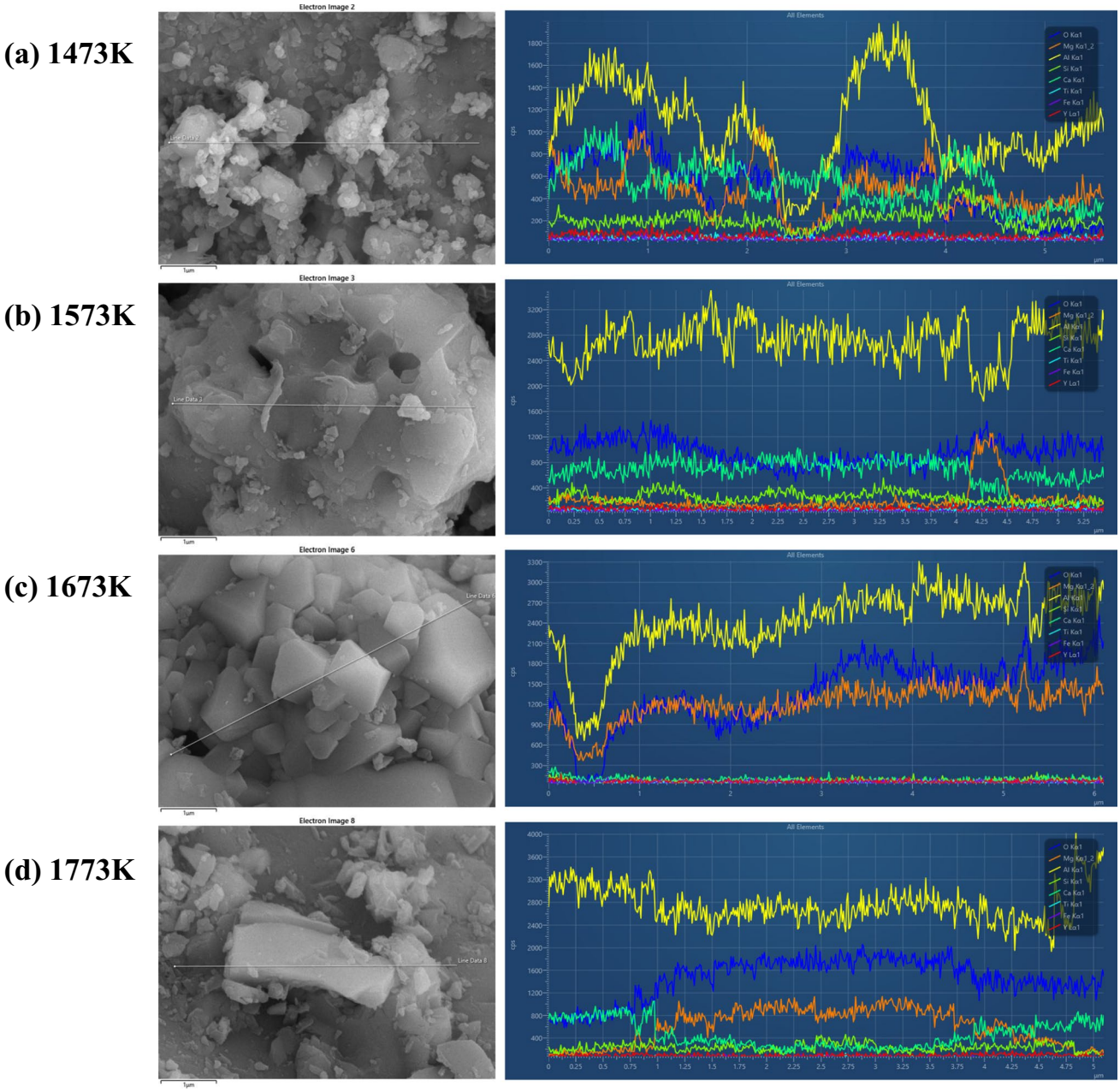

Fig. 6 SEM images and line scanning of the spinel powder with Y2O3 at different sintering temperatures for 3 h. **a** 1473 K. **b** 1573 K. **c** 1673 K. **d** 1773 K

Effect of Y_2O_3 dissolution and exsolution

With MDI Jade 5.0 software, the lattice cell refinement function can be used to calculate the lattice constant changes. From Table 3, the lattice parameters at different temperatures were higher than those obtained with refinement, which may be attributed to the dissolution of Y_2O_3 and other compounds such as CaO and SiO_2 [28, 29]. The lattice parameter of C_2AS increased at 1473 to 1573 K and decreased at 1673 K. The lattice parameter of MA increased at 1473 to 1673 K and decreased at 1773 K. Dissolution and exsolution were related to diffusion. Diffusion enhances intermolecular motion, which is good for the densification of materials [30].

Figure 9 illustrates the mechanism underlying the enhancement in the characteristics of the gehlenite/magnesia-alumina spinel derived from SAA after Y_2O_3 doping. The densification feature of the gehlenite/magnesia-alumina spinel was attributed to the low-viscosity liquid phase. The

Table 2 EDS analysis for the spinel powders with Y_2O_3 at 1473–1773 K for 3 h

Temperature/K	Element content (wt%)								
	O	Mg	Al	Si	Ca	Ti	Fe	Y	Possible phase
1473	40.4	10.3	25.6	4.6	18.2	0.4	0.5	–	–
1573	39.6	4.2	23.6	10.0	20.8	0.2	0.6	0.9	$YCaAl_3O_7$
1673	42.9	16.1	37.7	0.2	1.2	0.1	1.7	–	–
1773	47.8	6.7	34.0	2.4	0.1	0.9	–	–	–

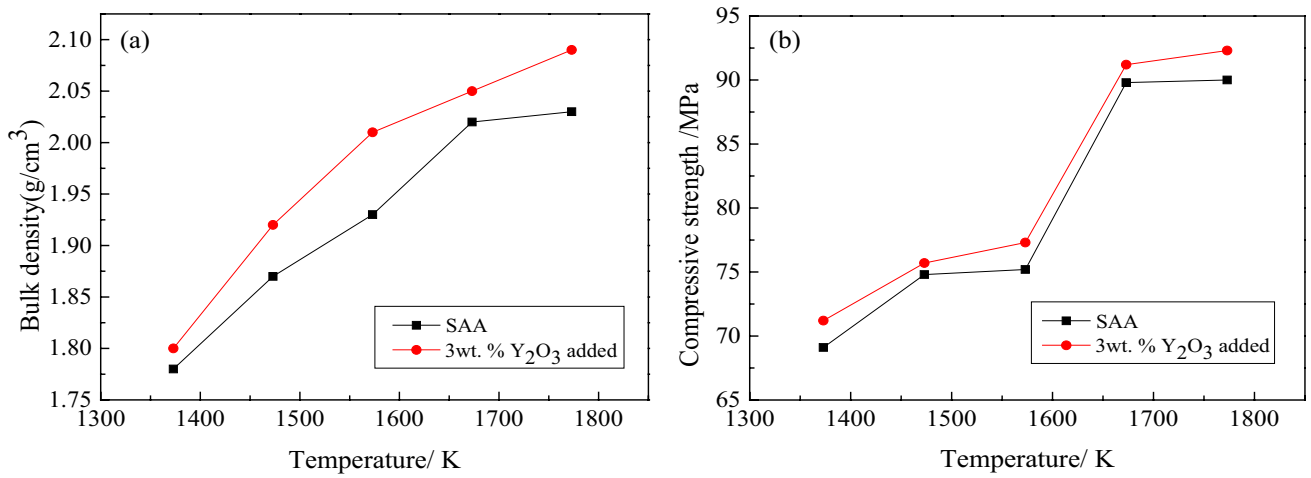

Fig. 7 Properties of the gehlenite/magnesia-alumina spinel with 3 wt% Y2O3 after sintering at different temperatures: **a** bulk density and **b** compressive strength

dissolution and exsolution of Y_2O_3 occurred in the sintering process. Schmid [31] and Su [32] reported that Y^{3+} was concentrated in the intergranular regions. The ionic radius of Y^{3+} was large than the ionic radii of Al^{3+}, Si^{4+}, Ca^{2+}, and Mg^{2+}. The solute misfit strain energy was obtained because of the other ionic radii of Y^{3+} and other ions. The predominant driving force for the segregation of Y^{3+} moved to the crystalline grain boundaries. Y^{3+} diffused into the anomalous microscopic defects and filled the crystalline grain boundaries during the high-temperature sintering process. Dissolution of Y ion in the sintering process resulted in cation vacancies that reinforced movement and mass transfer [30, 33]. The Y ion in other ion sites caused lattice strain, which also reinforced the mass transport process for densification [18, 30, 34]. Y_2O_3 moved to the ion boundaries and then entered the gehlenite/magnesia-alumina spinel lattice. Interionic migration decreased the residual pores in the MA and C_2AS boundaries and increased the density feature of the spinel. The Y_2O_3 can also reduce the coefficient of thermal expansion and the softening point of the glass phase. Several factors cooperatively enhance the characteristics of the gehlenite/magnesia-alumina spinel [35].

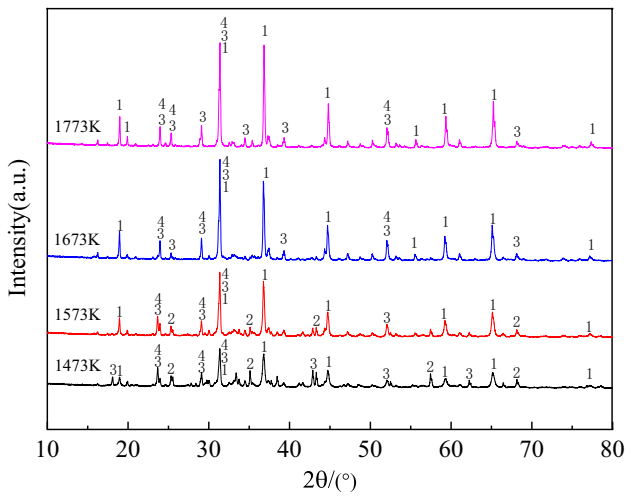

Fig. 8 XRD patterns of the gehlenite/magnesia-alumina spinel doped with 3 wt% Y2O3 at sintered at different temperatures for 3 h. 1-MgAl2O4; 2-Al2O3; 3-Ca2Al2SiO7; 4-YCaAl3O7

Table 3 Lattice constants (Å) of Y_2O_3-doped spinel at different sintering temperatures

Temperature/K	$Ca_2Al_2SiO_7$	$MgAl_2O_4$
Refine/Å	7.68580	8.08310
1473	7.69397	8.09246
1573	7.69863	8.09709
1673	7.69622	8.10043
1773	7.69354	8.08361

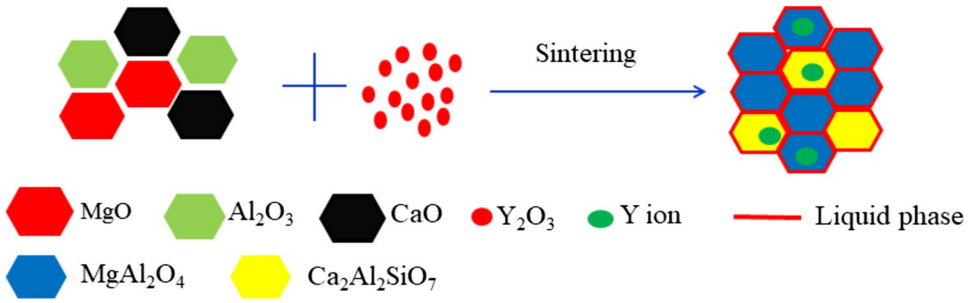

Fig. 9 Mechanism underlying the enhancement in the characteristics of the gehlenite/magnesia-alumina spinel derived from SAA after Y2O3 doping

Conclusions

Secondary aluminium ash (SAA) can be used as the raw material of gehlenite/magnesia-alumina spinels. The density of the bricks changed from 1.78 to 2.03 g·cm^{-3}, and the compressive strength changed from 69.1 to 90 MPa when they were sintered at a temperature ranging from 1373 to 1773 K for 3 h. The compressive strength of the gehlenite/magnesia-alumina spinel was above the Chinese national standard value of 40 MPa for magnesia and magnesia-alumina refractory bricks (GB/T 2275–2007). The density and compressive strength of the gehlenite/magnesia-alumina spinel doped with 3 wt% Y_2O_3 and sintered at 1673 K were 2.05 g·cm^{-3} and 91.2 MPa, respectively. The enhancing mechanism of Y_2O_3 doping contributed to the solubility of both Y_2O_3 and Y_2O_3-containing compounds, such as $YCaAl_3O_7$, which was turned into the low-viscosity liquid phase as the sintering temperature exceeded 1473 K.

Funding This work was supported by National Natural Science Foundation of P. R. China (Grants 52004113).

Declarations

Conflict of interest The authors declare no competing interests.

References

1. Hong, J.P., Wang, J., Chen, H.Y., Sun, B.D., Li, J.J., Chen, C.: Process of aluminum dross recycling and life cycle assessment for Al-Si alloys and brown fused alumina [J]. Trans. Nonferrous. Metals. Soc. China. **20**, 2155–2161 (2010)
2. Lopez-Delgado, A., Tayibi, H., Perez, C., Alguacil, F.J., Lopez, F.A.: A hazardous waste from secondary aluminum metallurgy as a new raw material for calcium aluminate glasses [J]. J. Hazard. Mater. **165**, 180–186 (2009)
3. Dmaschio, R., Fabbri, B., Fiori, C.: Industrial applications of refractories containing magnesium aluminate spinel [J]. Ind. Ceram. **8**, 121–126 (1988)
4. P E Tsakiridis. Aluminum salt slag characterization and utilization--a review [J]. J. Hazard. Mater. 2012: 217–218.
5. B Dash, B R Das, B C Tripathy, BHATTACHARYA I N, DAS S C. Acid dissolution of alumina from waste aluminum dross [J]. Hydrometallurgy. 2008, 92(1–2): 48–53.
6. David, E., Kopac, J.: Hydrolysis of aluminum dross material to achieve zero hazardous waste [J]. J. Hazard. Mater. **209–210**(4), 501–509 (2012)
7. Shinzato, M.C., Hypolito, R.: Solid waste from aluminum recycling process: characterization and reuse of its economically valuable constituents [J]. Waste Manage. **25**(1), 37–46 (2005)
8. Tan, R., Khoo, H.H., Chen, A.: Study of a primary aluminum supply chain [J]. J. Clean. Prod. **13**(6), 607–618 (2005)
9. Tavangarian, F., Emadi, R.: Synthesis and characterization of pure nanocrystalline magnesium aluminate spinel powder [J]. J. Alloy. Compd. **489**(2), 600–604 (2010)
10. Bonnefont, G., Fantozzi, G., Trombert, S., Bonneau, L.: Fine-grained transparent $MgAl_2O_4$ spinel obtained by spark plasma sintering of commercially available nanopowders [J]. Ceram. Int. **38**(1), 131–140 (2012)
11. Lv, C.S., Wang, J.W., Jia, Y.Z.: Effects of red mud content on the sintered red mud bricks [J]. J. Saf. Environ. **13**(4), 98–100 (2013)
12. Ma, J., Zhu, S.G., Di, P., Zhang, Y.: Influence of La_2O_3 addition on hardness, flexural strength and microstructure of hot–pressing sintered WC-MgO bulk composites [J]. Mater. Des. **32**(4), 2125–2129 (2011)
13. Qiu, G.M., Li, X.K., Qiu, T., Zhao, H.T., Yu, H.H., Ma, R.T.: Application of rare earths in advanced ceramic materials [J]. J. Rare Earths **25**(2), 281–286 (2007)
14. Kong, L.B., Zhang, T.S., Ma, J., Boey, F., Zhang, R.F.: Mullite phase formation in oxide mixtures in the presence of Y_2O_3, La_2O_3 and CeO_2 [J]. J. Alloy. Compd. **372**(1–2), 290–299 (2004)
15. Qu, H.X., Wu, Q., Wen, H.Q.: Effect of CeO_2 additives on the microstructure and mechanical properties of WC-Al_2O_3 composites [J]. Baosteel Tech. Res. **9**, 17–22 (2015)
16. Baranova, T.F., Kurskaya, I.N., Dabizha, N.A., Petrov, Y.B., Lukin, E.S.: Sintering high-purity fusions of MgO and MgO·Al_2O_3 [J]. Refractories **22**, 180–182 (1981)
17. Shi, Z.M., Pan, F., Liu, D.Y., Liang, K.M., Gu, S.R.: Effect of Ce^{4+}-modified amorphous SiO_2 on phase transformation towards α-cordierite [J]. Mater. Lett. **57**, 409–413 (2011)
18. Sarkar, R., Tripathi, H.S., Ghosh, A.: Reaction sintering of different spinel composition in the presence of Y_2O_3 [J]. Mater. Lett. **58**(16), 2186–2191 (2004)
19. Tian, Z.K., Wang, Z.F., Wang, X.T., Naihuo, C.: Effect of rare earth oxides on synthesis of magnesium aluminate spinel by reaction sintering [J]. Refractories **42**, 326–329 (2008)
20. Hasan, M., Dholabhai, P., Dey, S., Uberuaga, B.P., Castro, R.H.: Reduced grain boundary energies in rare-earth doped $MgAl_2O_4$ spinel and consequent grain growth inhibition [J]. J. Eur. Ceram. Soc. **37**, 4043–4050 (2017)
21. Suryanarayana, C.: Mechanical alloying and milling [J]. Prog. Mater. Sci. **46**, 1–184 (2001)

22. E M Vlad, R V Buzduga, M D Buzduga, V Caloian, E F Plopeanu, C Pandelescu, C Dobresc, N Constantin. Experimental research on the effect of additives on the sintering process of alumina-based refractory materials [J]. J. Phys. Confer. Ser. 2021, 1781(012066).
23. X P Tan, S Q Liang.Thermal phase transformation of SiO_2-Al_2O_3-ZrO_2 glass [J]. J. Central South Univ. (Science and Technology). 2011, 42(1).
24. P Y Yan, W Y Yang. Study on the cementitious behaviour of CaO Al_2O_3 SiO_2 glass [J]. J. Chin. Ceram. Soc. 1997, 25(4).
25. Ge, X.Z., Ge, Q., Ge, X.S., Ji, D.H., Huang, Y., Zhang, Z.L., Zhang, H.B.: Influence of La_2O_3 addition on microstructure and mechanical properties of Al_2O_3 ceramics [J]. Mater. Sci. Forum **956**, 69–77 (2019)
26. Fu, P., Xu, Z.J., Chu, R.Q., Li, W., Xie, Q.: Application study actuality and development foreground of rare earth oxides in ceramics materials [J]. Ceramics. **12**, 7–10 (2008)
27. Akin, I., Yilmaz, E., Sahin, F., Yucel, O., Goller, G.: Effect of CeO_2 addition on densification andmicrostructure of Al_2O_3–YSZ composites [J]. Ceram. Int. **37**, 3273–3280 (2011)
28. Naik, P.P., Tangsali, R.B.: Enduring effect of rare earth (Nd^{3+}) doping and γ-radiation on electrical properties of nanoparticle manganese zinc ferrite [J]. J. Alloy. Compd. **723**, 266–275 (2017)
29. Kim, T., Kim, D., Kang, S.: Effect of additives on the sintering of $MgAl_2O_4$ [J]. J. Alloy. Compd. **587**, 594–599 (2014)
30. Sarkar, R., Das, S.K., Banerjee, G.: Effect of additives on the densification of reaction sintered and presynthesised spinels [J]. Ceram. Int. **29**, 55–59 (2003)
31. Schmid, H.K., Pennefather, R., Meriani, S., Schmid, C.: Redistribution of Ce and La during processing of Ce(La)-TZP/Al_2O_3 composites [J]. J. Eur. Ceram. Soc. **10**, 381–392 (1992)
32. Su, C.H., Duanmu, Q.D., Wang, Y.: Non-equilibrium thermodynamic analysis of the concentration distribution of rare earth oxide at alumina transparent ceramic crystal boundary [J]. J. Chin. Ceram. Soc. **26**, 802–807 (1998)
33. Hirai, S., Murakami, H., Katayama, H.G.: Effect of additives on the formation of $MgAl_2O_4$ from MgO and Al_2O_3 [J]. J. Japan Inst. Metals. Mater. **55**, 166–171 (1991)
34. Skomorovskaya, L.A.: Magnesia spinel ceramics alloyed with rare earth oxides [J]. Glass Ceram. **50**, 165–168 (1993)
35. Wu, T.T.: Effect of rare earth oxides on the wear reaiatance and acid resistance of high-alumina ceramic [D]. Wuhan University of Technology, Wu Han (2017)